IEEE Access
Multidisciplinary | Rapid Review | Open Access Journal

Received June 28, 2020, accepted July 12, 2020, date of publication July 15, 2020, date of current version July 27, 2020.

Digital Object Identifier 10.1109/ACCESS.2020.3009380

Metasurface-Based Single-Layer Wideband Circularly Polarized MIMO Antenna for 5G Millimeter-Wave Systems

NIAMAT HUSSAIN, (Graduate Student Member, IEEE), MIN-JOO JEONG, ANEES ABBAS, AND NAM KIM

Department of Computer and Communication Engineering, Chungbuk National University, Cheongju 28644, South Korea

Corresponding author: Nam Kim (namkim@chungbuk.ac.kr)

This work was supported in part by the Information Communication Technology (ICT) Research and Development Program of Ministry of Science and Information Technology (MSIT)/Institute for Information and communications Technology Promotion (IITP) (A Study on Public Health and Safety in a Complex EMF Environment), South Korea, under Grant 2019-0-00102, and in part by Ministry of Science and Information Technology (MSIT)/Radio Research Agency (RRA) (Development of Rapid Antenna Measurement Technique for Antennas with New Radio Technology), South Korea.

ABSTRACT This paper presents a metasurface-based single-layer low-profile circularly polarized (CP) antenna with the wideband operation and its multiple-input multiple-output (MIMO) configuration for fifth-generation (5G) communication systems. The antenna consists of a truncated corner patch and a metasurface (MS) of a 2 × 2 periodic square metallic plates. The distinguishing feature of this design is that all the radiating elements (radiator and MS) are printed on the single-layer of the dielectric substrate, which ensures the low-profile and low-cost features of the antenna while maintaining high gain and wideband characteristics. The wideband CP radiations are realized by exploiting surface-waves along the MS and its radiation mechanism is explained in detail. The single-layer antenna geometry has an overall compact size of $1.0\lambda_0 \times 1.0\lambda_0 \times 0.04\lambda_0$. Simulated and measured results show that the single-layer metasurface antenna has a wide 10 dB impedance bandwidth of 23.4 % (24.5 – 31 GHz) (23.4 %) and overlapping 3-dB axial ratio bandwidth of 16.8 % (25 – 29.6 GHz). The antenna also offers stable radiation patterns with a high radiation efficiency (>95%) and a flat gain of 11 dBic. Moreover, a 4-port (2 × 2) MIMO antenna is designed using the proposed design by placing each element perpendicular to each other. Without a dedicated decoupling structure, the MIMO antenna shows an excellent diversity performance in terms of isolation between antenna elements, envelope correlation coefficient, and channel capacity loss. Most importantly, the operational bandwidth of the antenna covers the millimeter-wave (mm-wave) band (25 – 29.5 GHz) assigned for 5G communication. These features of the proposed antenna system make it a suitable candidate for 5G smart devices and sensors.

INDEX TERMS 28 GHz, metasurface antenna, fifth-generation (5G), millimeter-wave systems, MIMO, circular polarization.

I. INTRODUCTION

The fifth-generation (5G) new radio (NR) is one of the most discussed technologies nowadays. Due to the exponentially increasing demands for high data rates, low-latency, and limited bandwidth available in the microwave region, the 5G NR systems will be using millimeter-waves (mm-waves) especially from 24 – 100 GHz [1]. The 5G NR is expected to bring a revolution in our daily lives due to its seamless connectivity through modern technologies such as smart homes, smart factories, virtual reality, telemedicine, and automotive cars [2]. The frequency band allocation is a key factor in testing and modeling of the 5G communication scenarios. The world's major telecom companies, standardization organization, and government bodies are working hard in the standardization and deployment of the 5G wireless communication systems. The detailed mm-wave spectrum allocated for 5G NR is given in Figure 1, in which most of the countries are considering or have already chosen 26/28 GHz band for 5G NR [3], [4].

The design of antennas for the allocated mm-wave for 5G has received huge importance in recent years [5]. Due to the high propagation and atmospheric losses in mm-waves,

The associate editor coordinating the review of this manuscript and approving it for publication was Jinming Wen.

Countries	24 – 28 GHz band	37 – 40 GHz band	64 – 71 GHz band
Korea	26.5 – 29.5 GHz		
Japan	27.5 29.5 GHz		
Singapore	24.25 -26.5 GHz 26.5 – 27.5 GHz		
Canada	27.5 – 28.35 GHz	37 – 40 GHz	64 – 71 GHz
USA	24.75 – 25.25 GHz 27.5 28.35 GHz	37 – 40 GHz 47.2 – 48.2 GHz	64 – 71 GHz
UK	26 GHz		
Germany	26 GHz		
France	26 GHz		
Italy	26.5 – 27.5 GHz		
Sweden	26.25 – 27.5 GHz		
Finland	25.1 – 27.5 GHz		
China	24.75 – 27.5 GHz	40 – 43.5 GHz	

FIGURE 1. The global 5G NR mm-wave spectrum.

high-gain antennas are required for 5G systems. Although, the patch antennas provide the advantages of low-cost, planar structure, and easy design have the disadvantages of narrow bandwidth and low-gain. A lot of work has been done to increase performance in terms of gain and bandwidth of the patch antennas. By placing a superstrate above a patch with a separation of half-wavelength or quarter-wavelength, the gain of the antenna can be significantly increased. However, these designs have high-profiles and poor mechanical properties due to the presence of the air gap [6]–[8].

Moreover, multiple patch-substrates are stacked directly to achieve wideband operation as well as gain improvements [9], [10]. Such designs suffer from complex geometries and non-planar structures. Lens-coupled antennas in which a dielectric lens is placed on radiator especially at high-frequencies to focus the radiated beam [11], [12]. These antennas have the advantages of high gain and wideband characteristics but have low radiation efficiencies due to the losses in the thick dielectric material and bulky size.

The array antennas provide high gain to increase signal strength but have the same channel capacity as a single antenna (being fed with the single port) and are suffering from power losses in complex power divider networks [13], [14]. Dielectric resonator antennas (DRAs) are used to avoid the ohmic losses in conductors in mm-waves [15]–[17]. Compared to the DRAs in microwave frequencies, the size of the mm-wave DRA is very small, therefore the practical realization is the main concern.

Alternatively, metasurfaces (MSs) have been widely combined with patch and slot radiators due to their properties to manipulate the electromagnetic waves [18]. Basically, MSs are placed at an optimal position above or beneath the radiator for high gain and wideband operation [19]–[22]. Again, the gap between the radiator and the MS layer poses the aforementioned problems. Furthermore, radiators are sandwiched between the MS layer and ground plane without the air gap to improve performance keeping the planar structure of the antennas [23]–[30]. Even so, these configurations have the critical drawback of multiple-layers of the printed substrate (MS layer and radiator layer), which increases fabrication cost and complex design architecture.

Recently, antennas with a single printed layer using a primary radiator surrounded by parasitic elements/metasurfaces have been reported in the literature [31]–[36]. In these designs, every radiating element is printed on a single-layer but have low gain and limited bandwidth. Moreover, all these studies are at microwave frequencies.

On the other hand, the use of multiple-input-multiple-out (MIMO) both in transmitting and receiving ends provides multiple paths for data traffic, thus increases the data rate, capacity, spectral efficiency, and link reliability [37]. Therefore antennas with MIMO functionality is the key requirements for 5G technology and are presented in the literature [38]–[47]. Most of the antennas designed for 5G mm-wave (26/28 GHz) band are linearly polarized (LP). The LP antennas transmit only in a single direction while circularly polarized (CP) antennas propagate in two orthogonal directions with the same signal strength to offer the freedom of orientation for transmitting and receiving antennas. This is the reason, most of the antennas used in satellite/wireless communication (RFID tags, sensors, tracking devices, etc) have circular polarization. Additionally, CP antennas also offer immunity against prominent propagation losses, interferences, and multi-path distortions in mm-wave frequencies. It is evident from the literature review that a few works have been done in the design of CP MIMO antennas at the designated 5G frequency bands [48]–[50]. This is simply because of the design and realization challenges that are associated with the much smaller (few millimeters) physical size of the antenna. The connector size is comparable with the overall size of the antenna poses further restriction in the design freedom. The Fabry-Perot CP antennas with MIMO features for 5G [48], [49] provide high gain and isolation but have the large antenna profiles, complex designs, mechanical issues due to the air gap between superstrate and radiator. Also, the multiple layered substrates/FSS (frequency selective surfaces) causes difficulty in the design realization and are not suitable for mass production for practical applications. A dual-band CP MIMO antenna with twelve ports for the 5G base stations is proposed in [50]. The antenna system provides both LP and CP radiations based on end-user requirements and the single-element antenna has a gain of 8 dBic with an AR bandwidth of only 3% (27.5 – 28.5 GHz).

Thus, it can be concluded that none of the reported antennas in literature has the advantages of wide bandwidth, CP, and MIMO features as well as the single-layer design at the same time. Therefore, a low-profile CP MIMO antenna covering the allocated 5G frequency band is the need of the time. Keeping the above considerations in mind, a single-layer CP antenna based on MS and its MIMO characterization for 5G communication systems is proposed. The antenna element consists of a truncated corner patch radiator surrounded by a MS of periodic square metallic plate unit cells. Most importantly, all radiating elements (patch and MS) are printed on a single dielectric substrate for low-profile, low-cost, and mass production suitability while maintaining high gain and wideband characteristics. The wideband CP radiations are realized by exploiting surface-waves along the MS. Moreover, a 2 $\times$ 2 MIMO antenna system is designed using the proposed

single-element antenna by placing each element perpendicular to each other showing excellent diversity performances. The main contributions of this work can be characterized as:

- To the best of the author's knowledge, it is the only available planar antenna with a single-layer for the 5G mm-wave band offering the advantages of CP and MIMO characteristics at the same time.
- The antenna has an extremely low height profile (0.51mm) being designed on a single-layer of the substrate with minimum parts of the assembly that offers low-cost and mass production suitability for practical applications.
- The operating bandwidth of the proposed single-layer CP MIMO antenna covers the frequency (25 – 29.5 GHz) band allocated for 5G communications with good radiation characteristics and excellent diversity performance (isolation, envelope correlation coefficient, diversity gain, and channel capacity losses) without a dedicated decoupling structure.

All the antenna simulations are done using CST Microwave Studio. The rest of the paper organization is as follows. The antenna geometry of the proposed single-element antenna, its design methodology, radiation mechanism, and simulated/measured results are presented in Section II. While the design of the MIMO configuration and its diversity parameters along with its performance comparison with state-of-the-art works is discussed in Section III. Finally, the proposed work is concluded in Section IV.

II. DESIGN AND FABRICATION OF THE SINGLE-ELEMENT ANTENNA

In this section, the design, characteristics as well as the radiation mechanism of the proposed single-element wideband CP antenna is explained.

A. ANTENNA GEOMETRY

The schematics of the proposed single-element CP antenna is shown in Figure 2. The antenna consists of a truncated corner square patch radiator and a MS lattice of periodic square metallic plates, both are printed on a single-layer of a low dielectric constant high-frequency substrate (Rogers 5880LZ, $\varepsilon_r = 2.0, tan\delta = 0.0009$). The patch is fed by an inset feed by extending the pin of the connector through a hole of 0.65 mm diameter, while the out conductor is soldered with the ground. The MS cells have periodicity P and the separation between the adjacent cells is g and are patterned around the patch for performance enhancement. Since all the radiating elements are printed in a single-layer, resulted in an extremely low-profile of the antenna (0.51 mm $\approx 0.041\ \lambda_0$), suitable for the compact 5G smart devices. The antenna has an overall size of only 12 mm × 12 mm × 0.51 mm which corresponds to $1.0\lambda_0 \times 1.0\lambda_0 \times 0.04\lambda_0$, where λ_0 is the free-space wavelength at lowest resonating frequency. The parameters for the optimum performance of the antenna are: $A = 12.4$, $h = 0.51$, $w = 3.4$, $g = 0.4$, $p = 2$, $w_F = 0.9$, and $t_c = 0.9$ (unit = mm).

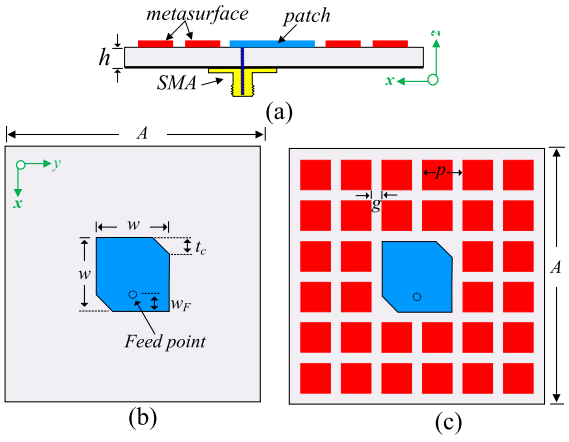

FIGURE 2. Antenna geometry: (a) side view of antenna, (b) top view of patch, and (c) top view of the patch with MS.

B. ANTENNA DESIGN PROCEDURE

The proposed single-layer 5G antenna based on MS evolved from an inset fed square patch antenna chosen to operate at the desired frequency of $f_r \sim 27$ GHz.

The initial patch dimension (w) may be predicted as:

$$w = \frac{c}{2f_r\sqrt{\varepsilon_{eff}}} \tag{1}$$

where c is the light velocity and ε_{eff} is the effective dielectric constant of the substrate. The antenna is fed from the bottom through a coaxial feed to avoid the connector effects. Basically, the square patch antennas have LP radiation. Among the conventional techniques, one of the easy ways to produce CP is the truncation of the corners [29]. A set of diagonal corners of the patch are truncated. This truncation (t_c) is tuned to adjusts the value of phase and magnitude of the two orthogonal modes for the realization of CP. It is well known that the single feed patch antennas have a limited impedance ($|S_{11}|$) and axial ratio (AR) bandwidths.

In order to improve the antenna performance, a MS made up of a periodic lattice of square metallic plates are patterned around the truncated patch antenna. The metasurface acts as a secondary radiating source by producing extra resonances both in $|S_{11}|$ and AR.

The simulated $|S_{11}|$ and AR of the corner truncated patch antenna with and without MS is shown in Figure 3. As expected, the antenna without MS has a narrow $|S_{11}|$ and AR bandwidths of 5 % and 2.5 %, respectively with only one minimum axial ratio point. However, the MS significantly improved the bandwidth of the antenna. The antenna with MS shows a wide $|S_{11}|$ bandwidth of 23.4 % and 16.8 % AR bandwidth.

The gain of the antenna with and without metasurface is shown in Figure 4. The gain of the antenna without metasurface is noted to be 7 dBic, while the gain with metasurface is increased up to 11.3 dBic due to the increased aperture efficiency of the antenna thanks to the metasurface.

Thus, a single-layer, wide bandwidth, and high gain CP antenna is designed. The detailed design procedure of the

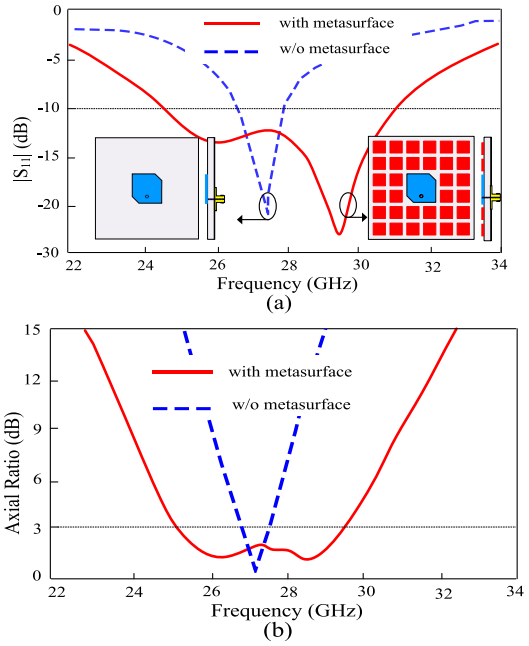

FIGURE 3. Characteristics of the proposed single-element antenna with and without metasurface: (a) $|S_{11}|$ and (b) axial ratio.

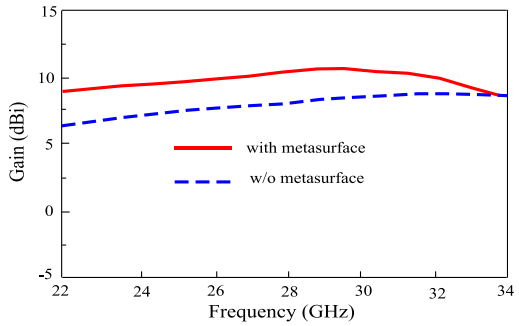

FIGURE 4. Gain of the proposed single-element antenna with and without metasurface.

single-element antenna is shown in Figure 5. The flow-chart explains the key design parameters and their impact on antenna characteristics ($|S_{11}|$, AR, and gain). Based on the flow chart, the optimization procedure for the proposed antenna can be summarized as follow.

1) DESIGN THE CP PATCH ANTENNA

The patch size (w) is chosen about half-effective wavelength at the resonating frequency and fed near corner for impedance matching. A coaxial feed is used to avoid connector effects. A set of corners are truncated by a factor t_c and optimized for CP radiation.

2) DESIGN OF SINGLE-LAYER CP ANTENNA WITH MS

An array of MS cells is patterned around the radiator in the same substrate layer and its dimensions (p, g) are tuned for

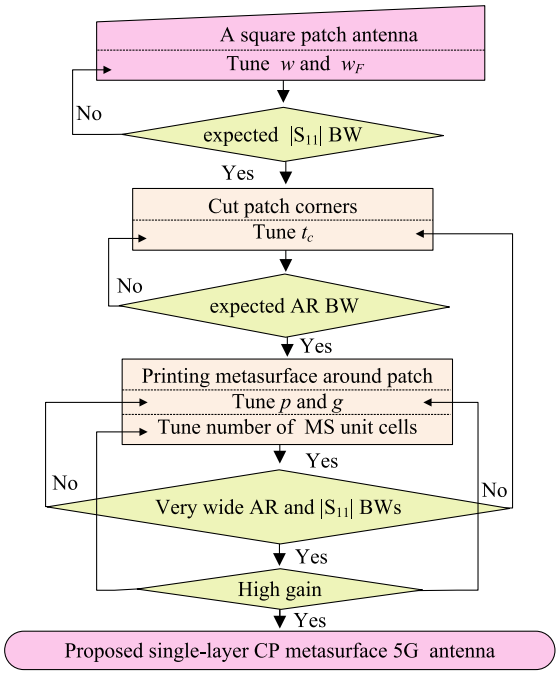

FIGURE 5. The design procedure and optimization of the proposed single-layer CP metasurface antenna.

wideband operation. A proper number of MS unit cells and its optimization resulted in gain enhancement.

C. RADIATION MECHANISM

The sub-wavelength two-dimensional periodic structures known as MS have been widely used for antenna's performance enhancement by exploiting surface wave resonances [26]–[29]. These designs consist of two separately printed layers, the MS layer and the patch radiator layer. The MS layer was directly stacked above the radiator to reduce the antenna height. The proposed single-layer CP antenna is based on these studies [26]–[29], where the antenna performance is improved by employing a MS of periodic square metallic plates to excite surface waves propagating along the MS for extra resonances. The propsed MS also achieve extra resoannces both in $|S_{11}|$ and AR profiles as shown previously in Figure 3. Unlike the prior designs, the MS unit cells are printed on the same dielectric layer as the corner truncated patch radiator to avoid the critical problems associated with two-layered antenna geometries, i-e high-profile, high-cost, and design complexity.

The surface wave resonances depend on the number (n) and periodicity (p) of MS unit cells, which can be computed by the transmission-line model as [30]:

$$\beta_{sw} = \frac{\pi}{L_{cav}} \tag{2}$$

$$L_{cav} = \mathrm{p} \times \mathrm{n} \tag{3}$$

Here, β_{sw} is the propagation constant and L_{cav} is the total length of the MS cavity [26]. A conceptual diagram of the surface wave propagation along a finite size MS is shown in

the inset of Figure 6. The propagation constant of transverse electric (TE) and transverse magnetic (TM) waves can be computed by [29]:

$$\beta_{TE} = \frac{\omega}{c}\sqrt{1 - \frac{(Z_{MS})^2}{(Z_0)^2}} \tag{4}$$

$$\beta_{TM} = \frac{\omega}{c}\sqrt{1 - \frac{(Z_0)^2}{(Z_{MS})^2}} \tag{5}$$

Here, ω is the angular frequency and c is the light velocity. While Z_{MS} represents the surface impedance of the metasurface and the free space impedance is denoted by Z_0.

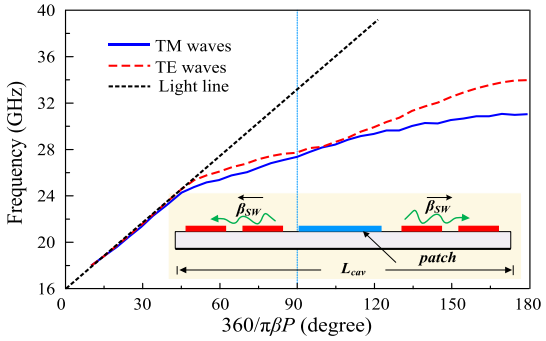

FIGURE 6. Concept of surface wave propagation and dispersion diagram of the proposed metasurface.

The dispersion curves of the unit cell are computed and plotted in Figure 6. For the phase shift of 90°, the intersection between dispersion lines and the vertical line shows the solution of equation (5), which represents the resonance point of the MS. For the proposed configuration, the surface waves are predicted to resonate around 28 GHz. Here, only the first two eigenmodes (TE and TM) are shown because these dominant modes have good broadside radiation based on the work done in [26]–[29]. It is noted that these studies used 4 × 4 unit cell MS, while we used 6 × 6 unit cells to compensate the removed unit cells to print radiator and the MS in the same layer.

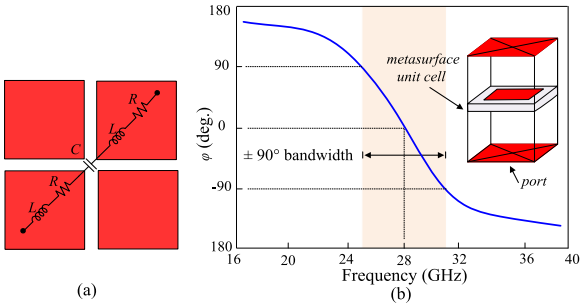

FIGURE 7. Characteristics of MS unit cells: (a) equivalent circuit diagram and (b) reflection phase.

The MS equivalent circuit diagram of the MS and its reflection phase characteristics are also investigated and shown in Figure 7. The MS can be represented by a series resonant RLC circuit [Fig. 7(a)]. The impedance Z_{MS} of the equivalent RLC circuit can be expressed as:

$$Z_{MS} = R + j\left(\omega L - \frac{1}{\omega C}\right) \tag{6}$$

The capacitance C is due to the E-field between the gapes of two adjacent square metallic plates. The inductance I is because of the current flowing on the unit cell, while R is the unit cell's own resistance.

Furthermore, the reflection phase φ of the unit cell obtained through full-wave simulation shows the in-phase reflections like high impedance surface (*HIS*) for an incident wave for a wide range of frequency bands (Figure 7(b)), suggesting the broadband operation of the proposed MS [26]. In general, the φ for *HIS* varies between +180° to –180° and gives zero value at a single frequency. This phenomenon lays the fundamental support in the design of the single-layer antenna, since the parallel image currents appear in-phase. Thus, the efficient radiations of the *HIS* placed on the same plane as the radiator is possible. The proposed unit cell gives 0° resonance at 28 GHz, while the in-phase bandwidth (± 90°) ranges from 25 to 31.8 GHz. In summary, the radiation characteristics of the proposed MS used in the design of the single-layer antenna are endorsed by the reflection phase characteristics and can be satisfactorily explained using the transmission-line model.

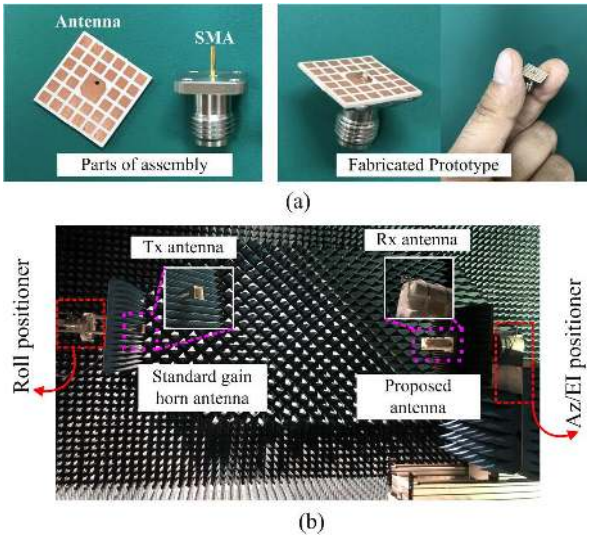

FIGURE 8. Photographs of the (a) fabricated antenna and its parts of the assembly, and (b) far-field measurement setup.

D. RESULTS AND DISCUSSION

To verify the design concept, a prototype of the proposed single-layer wideband CP antenna is fabricated on a high-frequency substrate (Rogers 5880, thickness = 0.51 mm) through photolithography with a high precision level of 0.05 mm and tested for measurement results. The photographs of the prototype and far-field measurement setup are shown in Figure 8. The pin of the mm-wave 2.92 mm K-connector is extended up to the patch through a hole

of 0.6 mm diameter. The $|S_{11}|$ is measured using PNA network analyzer (Agilent Technologies E8364B) in open-air condition. The far-field measurements are done at the anechoic chamber [56]. A standard gain horn antenna is used as a transmit antenna and the prototype is measured as a receiving antenna. Amplifiers were used to supply stable power reception. The antenna under test is rotated to measure the radiation intensity at different orientations. Owing to its single-layer geometry, there are no issues of misalignment due to the minimum parts for assembly. Therefore a good agreement between the numerically computed and measured results are observed.

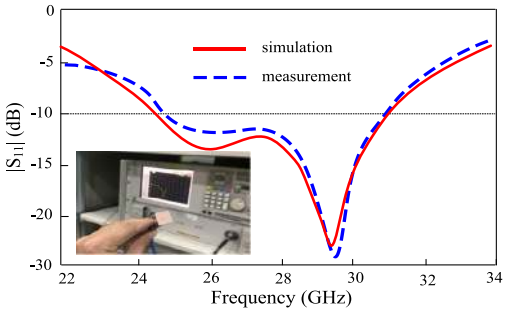

FIGURE 9. Simulated and measured $|S_{11}|$ of the proposed single-layer 5G metasurface antenna.

1) $|S_{11}|$ CHARACTERISTICS

The simulated and the measured $|S_{11}|$ of the proposed single-element antenna is depicted in Figure 9. It observed that the antenna offers a good impedance matching ($|S_{11}| < -10$ dB) for a wideband frequency starting from 24.5 to 31 GHz corresponds to a fractional bandwidth of 23.4 % with respect to the central frequency. The wideband characteristics are thanks to the successful implementation of MS.

2) AR, GAIN, AND RADIATION EFFICIENCY

The radiation characteristics of the single-element antenna in terms of AR, broadside gain, and radiation efficiency are shown in Fig. 10. The antenna has a wide 3-dB AR bandwidth (16.8 %) with several minimum AR points ranging from 25 to 29.6 GHz with a flat gain curve and a high simulated (both with CST and HFSS) radiation efficiency of more than 95 %. Again, wideband and high gain characteristics are due to the usage of MS as a secondary radiator for useful extra resources. The measured gain achieved a maximum value of 11 dBic with minimum fluctuations satisfying the high gain requirements for 5G mm-wave communication systems. The measured gain is little lower than the simulated values in the entire frequency range due to connector/cable losses used during measurement. It is worth noting that the AR bandwidth is overlapped within the $|S_{11}|$ bandwidth and the common bandwidth of the antenna covers the allocated frequency bands for 5G systems.

3) RADIATION PATTERNS

The radiation patterns of the antenna in E- and H-plane at different operating frequencies are shown in Figure 11.

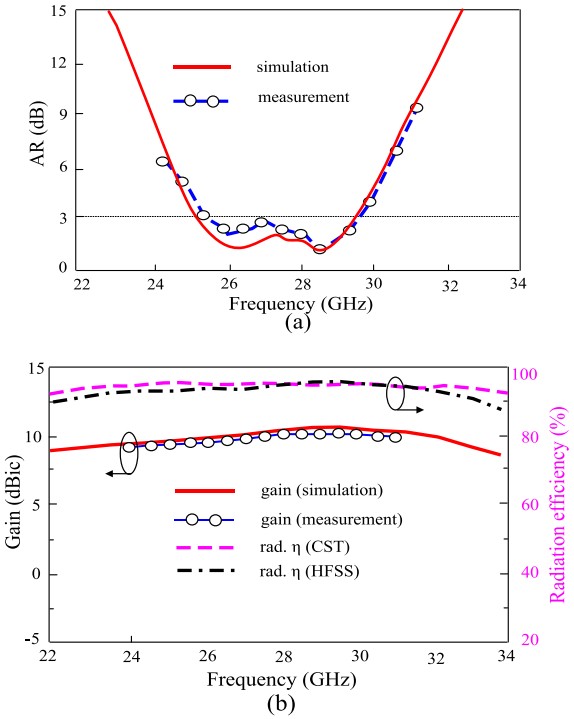

FIGURE 10. Simulated and measured (a) axial ratio and (b) broadside gain and radiation efficiency of the proposed single-layer 5G metasurface antenna.

The antenna offers stable and symmetrical radiation patterns having low side-lobe and back-lobe levels at all the investigated frequencies of 25, 28, and 31 GHz in the passband. It is observed that the left-hand CP (LHCP) is negligible compared to the right-hand CP (RHCP). Thus the antenna has RHCP in broadside direction ($\theta = 0°$). The polarization of the antenna is further explained by looking at the E-field from +z-direction (Figure 12). The E-field at two minimum AR points (26 and 28.5 GHz) for various values of ω_t(ω_t=0°, ω_t=90°, and ω_t=180°) rotates in a counter-clockwise direction proving the RHCP of the proposed single-layer MS 5G antenna.

III. DESIGN AND FABRICATION OF THE PROPOSED MIMO ANTENNA

Due to the increasing demands of smart devices and IoTs, the design of the CP MIMO antennas at 5G bands is highly desirable to provide fast-data rates, improve capacity, and link reliability. Moreover, there is not a single CP MIMO antenna reported in the literature with a single printed layer

configuration. Therefore, the single-element antenna design is incorporated into a 4-port (2 × 2) MIMO system.

A. MIMO ANTENNA GEOMETRY

The MIMO consists of 4-single element antennas placed orthogonal to each other and is simply designed by translating the single-element at 90° without changing any design parameter except the overall size of the shared substrate as shown in Figure 13. The distance between the two adjacent

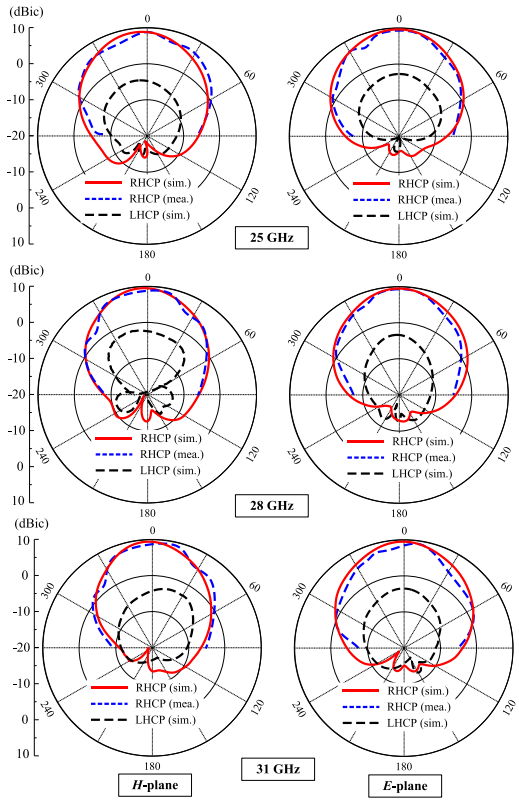

FIGURE 11. Radiation patterns of the proposed metasurface antenna at different frequencies.

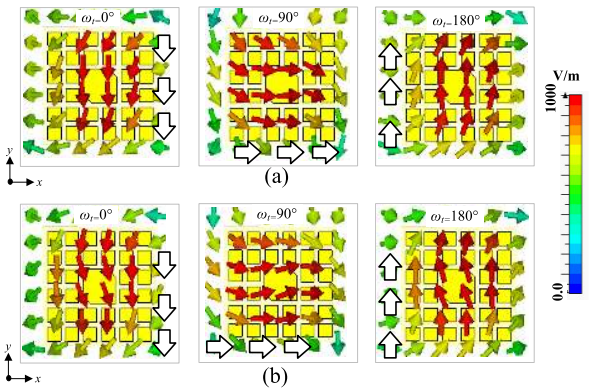

FIGURE 12. Rotating E-field of the proposed antenna: (a) 26 GHz and (b) 28.5 GHz.

MIMO elements is $(2 \times p) + g$, which is actually the distance between patch edge to the substrate edge in the single-element antenna. This arrangement ensures the simple MIMO geometry.

B. RESULTS AND DISCUSSION

The MIMO antenna is fabricated for measurement results as shown in Figure 14. The MIMO diversity performance in terms of isolation, envelope correlation coefficient, diversity

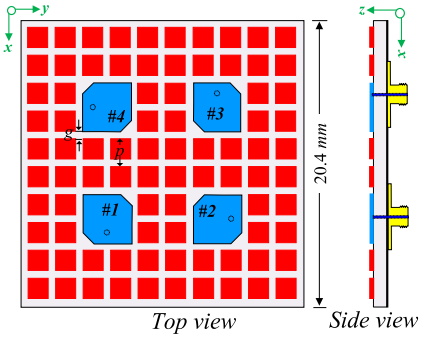

FIGURE 13. The geometry of the proposed MIMO antenna.

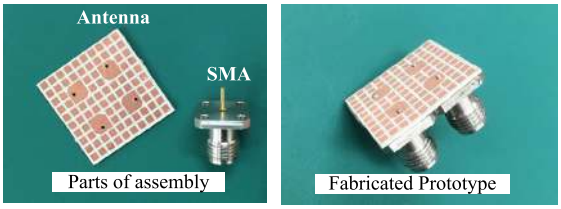

FIGURE 14. The geometry of the proposed MIMO antenna.

gain, and channel capacity loss are studied to show the robustness of the MIMO antenna system.

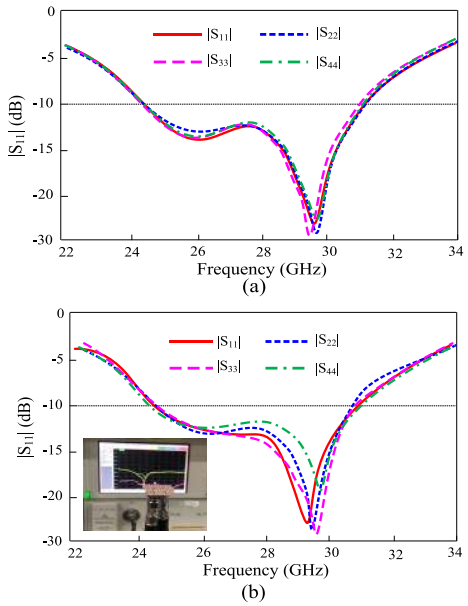

FIGURE 15. Reflection coefficients of the proposed MIMO antenna: (a) simulated and (b) measured.

1) REFLECTION COEFFICIENTS

Figure 15 shows the simulated and the measured reflection coefficient plots of the CP MIMO antenna. Since all the antenna elements have symmetrical geometry and placement, the antennas show almost the same reflection coefficients curves. The MIMO antennas have a similar 10 dB bandwidth

(24.5 to 31 GHz) as the proposed single-element antenna. A little difference in the measured reflection coefficients among the antenna elements are due to the soldering.

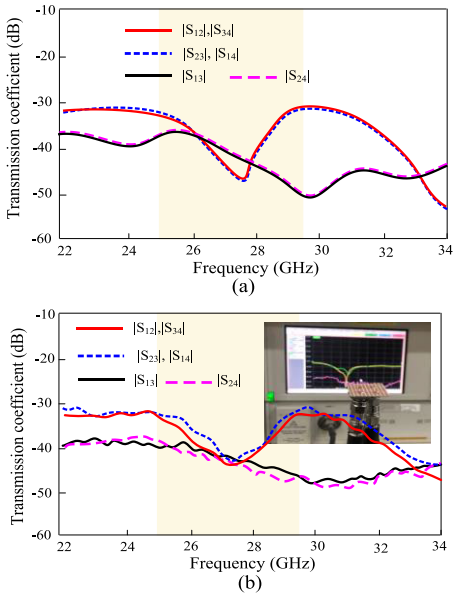

FIGURE 16. Transmission coefficients of the proposed MIMO antenna: (a) simulated and (b) measured.

2) TRANSMISSION COEFFICIENTS

The mutual coupling between the MIMO elements can be expressed by the transmission coefficient. The measured and simulated transmission coefficients are plotted in Figure 16. The antennas shows a high isolation characteristics without a dedicated decoupling structure. Even the separation between the antenna elements is only $0.36\lambda_o$ (4.4 mm), the antennas minimum isolation is <-30 dB in the entire operating bandwidth. This is due to the MS unit cells present between the adjacent antennas, which serve as the decoupling structure. The mechanism of coupling reduction between MIMO elements placing periodic structures between the antenna elements is well explained in [41], [55]. The transmission coefficient for $|S_{12}|$, $|S_{14}|$, $|S_{23}|$, and $|S_{34}|$ show identical curves due to the symmetrical geometry of the respective antennas. Moreover, the $|S_{13}|$ and $|S_{24}|$ curves are the same with lower values (<-35 dB), since these antennas are located at the diagonal positions having longer distance among them compared to other adjacent antennas.

3) ENVELOPE CORRELATION COEFFICIENT

The envelope correlation coefficient (ECC) shows how much MIMO antennas are independent in their individual performance, for instance, radiation patterns and polarization. The ECC (ρ_{eij}) for the MIMO antenna system can be computed using both the S-parameters and far-field radiation patterns using (7) and (8), respectively [47].

$$\rho_{eij} = \frac{|S_{ii}^* S_{ij} + S_{ji}^* S_{jj}|^2}{(1 - |S_{ii}|^2 - S_{ij}^2)(1 - |S_{ji}|^2 - S_{jj}^2)} \tag{7}$$

$$\rho_{eij} = \frac{\left| \iint_{4\pi} \left[\vec{R}_i(\theta, \varphi) \times \vec{R}_j(\theta, \varphi) \right] d\Omega \right|^2}{\iint_{4\pi} \left| \vec{R}_i(\theta, \varphi) \right|^2 d\Omega \iint_{4\pi} \left| \vec{R}_j(\theta, \varphi) \right|^2 d\Omega} \tag{8}$$

where S_{ii} is the reflection coefficient and S_{ij} is the transmission coefficient. Ω is the solid angle and $\vec{R}_i(\theta, \varphi)$ and $\vec{R}_j(\theta, \varphi)$ are the three-dimensional radiation patterns of i^{th} and j^{th} antenna, respectively. The ECC values obtained from (7) and (8) for the proposed CP MIMO antenna are very low (0.015) within the operating frequency, showing the excellent diversity performance and uncorrelated far-field patterns of the MIMO antennas (Figure 17). The simulated 3D radiation patterns of the MIMO antennas is also suggesting that the antennas are independent in their individual performance as the radiation patterns do not deteriorate in MIMO configuration (Figure 18).

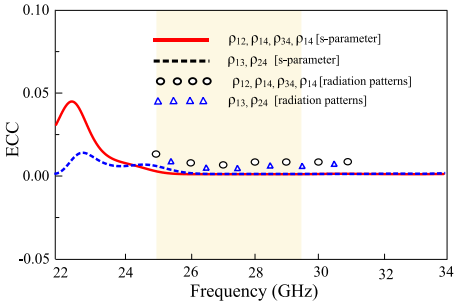

FIGURE 17. ECC of the proposed MIMO antenna.

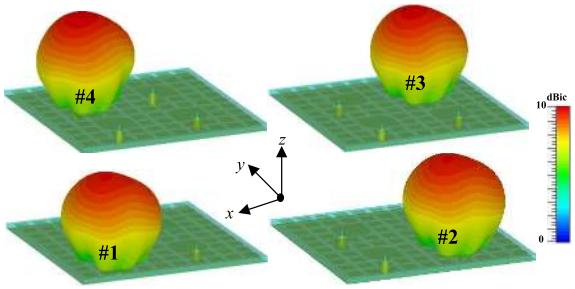

FIGURE 18. Simulated radiation patterns of the proposed MIMO antennas at 28 GHz.

4) DIVERSITY GAIN

The diversity gain (DG) is an another fundamental parameter that describes the effect of diversity scheme on the radiated power. DG of the proposed MIMO is computed as a function of frequency using the relation in (9) and shown in Figure 19.

$$\mathrm{DG} = 10\sqrt{1 - |\rho_{\mathrm{eij}}|^2} \tag{9}$$

The diversity gain for all the antenna elements is more than 9.91 dB which is very close to the ideal value of 10 dB.

TABLE 1. Comparison of the proposed single-layer CP 5G MIMO antenna with state-of-the-art works.

Refs.	Antenna type	Antenna profile (λ_0)	f_c (GHz)	LP/CP	-10dB $\|S_{11}\|$ BW (%)	3dB AR BW (%)	Max. Gain	Printed layers	Air gap	MIMO features
[26]	Patch + metasurface	0.093	27.5	CP	34.7	20.1	11 dBic	2	No	No
[34]	Patch + metasurface	0.04	5.7	CP	18	12.8	8.4 dBic	1	No	No
[35]	Patch + parasitic	0.01	2.5	CP	Not given	15.8	Not given	1	No	No
[36]	Patch + parasitic	0.016	3.05	CP	6	3.3	2.7 dBic	1	No	No
[44]	Patch + DGS	0.07	28	LP	14.6	-	8.3 dBi	1	No	Yes
[45]	Patch + EBG	Not given	24	LP	3.0	-	6 dBi	1	No	Yes
[46]	Patch + DGS	0.13	25.2	LP	15.6	-	8.7 dBi	1	No	Yes
[47]	Patch + DGS	0.06	31	LP	39	-	10.6 dBi	1	No	Yes
[48]	Patch + superstrate	0.35	30	CP	19	6	8 dBic	3	Yes	Yes
[49]	Patch + superstrate	0.7	28	CP	27.6	17	14.1 dBic	2	Yes	Yes
[50]	Vivaldi antenna	0.5	28/38	CP/LP	6	3	8 dBic	1	No	Yes
[51]	Yagi Uda + EBG	0.36	29	CP	19	10	11.9 dBic	3	No	No
[52]	Dipole + SRR	0.27	29.5	CP	17.2	10	11.9 dBic	2	Yes	No
[53]	Dielectric resonator	0.12	25	CP	34	30	8.1 dBic	04	No	No
[54]	Cross dipole	0.15	28	CP	8	8	2.2 dBic	1	No	No
Prop.	**Patch + metasurface**	**0.04**	**27.5**	**CP**	**23.4**	**16.8**	**11 dBic**	**1**	**No**	**Yes**

DGS stands for defected ground structures, *EBG* stands for electromagnetic bandgap, *SRR* stands for split ring resonator, λ_0 is free space wavelength at resonance frequency, and f_c is the center frequency.

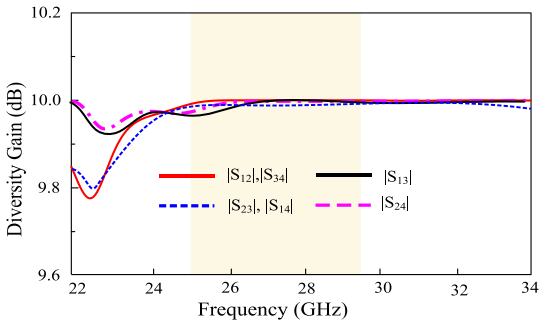

FIGURE 19. Diversity gain of the proposed MIMO antenna.

5) CHANNEL CAPACITY LOSS

One of the critical parameters in MIMO systems is the channel capacity loss (CCL). The correlation in MIMO links may reduce MIMO capacity. The CCL may be calculated using (10a) [47].

$$C\,(loss) = -log_2 \det\,(M_{ANT}) \tag{10a}$$

where M_{ANT} is the correlation matrix,

$$M_{ANT} = \begin{bmatrix} \alpha_{11} & \alpha_{12} & \alpha_{13} & \alpha_{14} \\ \alpha_{21} & \alpha_{22} & \alpha_{23} & \alpha_{24} \\ \alpha_{31} & \alpha_{32} & \alpha_{33} & \alpha_{34} \\ \alpha_{41} & \alpha_{42} & \alpha_{43} & \alpha_{44} \end{bmatrix} \tag{10b}$$

where

$$\alpha_{ii} = 1 - \left| \sum_{n=1}^{n=4} S_{in}^{*} S_{ni} \right|, \quad for\ i, j = 1, 2, 3, or\ 4. \tag{10c}$$

and

$$\alpha_{ij} = - \left| \sum_{n=1}^{n=4} S_{in}^{*} S_{nj} \right|, \quad for\ i, j = 1, 2, or\ 4. \tag{10d}$$

The CCL in the proposed MIMO antenna is computed using [10(a-d)] and plotted in Figure 20. The CCL is noted to be very low, i-e less than 0.19 bits/s/Hz in the operating bandwidth, which shows the proposed MIMO antenna's high throughput.

C. PERFORMANCE COMPARISON

The proposed single-layer 5G MIMO antenna is compared in terms of the overall height profile, bandwidth ($|S_{11}|$ and AR), gain, design simplicity (number of printed layers and presence of air gap), and MIMO functionality with the existing state-of-the-art designs in the literature in Table 1. For a fair comparison, the antenna type (the technique used in performance enhancement) and operating frequencies are

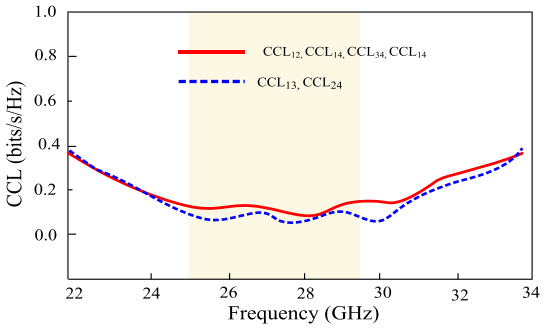

FIGURE 20. Channel capacity loss of the proposed MIMO antenna.

TABLE 2. Comparison of the proposed MIMO antenna with other mm-wave MIMO antennas.

Refs.	Element spacing	Minimum Isolation (dB)	ECC	CCL (bits/s/Hz)
[44]	Not given	17	0.01	0.4
[45]	$0.41\lambda_o$	37	0.24	Not given
[46]	$0.84\lambda_o$	16.2	Not given	Not given
[47]	$1.06\lambda_o$	22	0.02	Not given
[48]	$0.5\lambda_o$	20	Not given	Not given
[49]	$0.6\lambda_o$	25	0.01	Not given
[50]	Not given	16	Not given	Not given
Prop.	$\mathbf{0.36\lambda_o}$	**30**	**0.015**	**0.19**

also included. It can be observed from the table that only the proposed antenna offers all the advantages of single-layer, low-profile, wide bandwidths, CP, and MIMO functionality at the 5G mm-Wave frequency band. The antennas reported in [34]–[36] offer the advantages of a single printed layer and CP radiations but have the disadvantages of limited AR bandwidths and the absence of MIMO functionality as well as low gain even though these designs are at microwave frequencies. It is worth mentioning that among the 5G antennas with MIMO capabilities [44]–[51], only [48]–[50] have CP polarization. The antennas with superstrate [48], [49] offer the advantages of MIMO, wide bandwidth, and high gain (<14 dBic) have the critical disadvantages of design complexity because of the multiple printed layers and the presence of air gap. The CP MIMO antenna presented in [50], has a low gain of 8 dBic while the CP bandwidth is restricted to only 3%. The 5G CP antennas presented in [26], [51]–[54] are missing MIMO features besides of limited operating bandwidths. Although [26] and [53] are offering wider operating bandwidths but have drawbacks of multiple printed layers. In addition, the MIMO matrics (isolation, ECC, and CCL) of the proposed antenna system with other MIMO antennas for 5G mm-Wave applications is compared in Table 2. Even though the spacing among the antenna elements (edge to edge) in our design is $\mathbf{0.36\lambda_o}$ has the minimum isolation of more than 30 dB in the entrie bandwidth as well as low ECC and CCL values. The high isolation characteristics of this design are thanks to the arthogonal arrangement of the antennas as well as the MS unit cells present among the adjacent antennas which are acting as decoupling structure. Therefore, it can be concluded that the proposed antenna outperforms the existing antennas with the advantages of its simple single-layer design, wide ($|S_{11}|$ and AR) bandwidths, and high gain (11 dBic) with its excellent MIMO functionality.

IV. CONCLUSION

A metasurface-based wideband CP MIMO antenna with a single-layer configuration having low-profile and low-cost characteristics for 5G mm-wave applications is presented. Both the CP radiator and the periodic metallic plate MS are printed on the same dielectric layer to achieve the performance enhancements. The radiation mechanism of the antenna is explained in depth through reflection phase characteristics and as well as the transmission-line model. The fabricated single-element antenna has a compact size of $1.0\lambda_0 \times 1.0\lambda_0 \times 0.041\lambda_0$. The antenna exhibits a wideband operational bandwidth from 25 to 31 GHz for $|S_{11}| < -10$ with an overlapping AR bandwidth of 16.8 % (25 – 29.6 GHz). Moreover, stable radiation patterns with little gain variations from 9.5 – 11 dBic are also achieved across the operating band. In addition, the proposed single-element antenna is characterized for 2 × 2 MIMO system by translating each antenna element perpendicular to each other. The MIMO antenna offers good diversity performance showing high isolation between antenna elements (< -30 dB), low envelope correlation coefficient (0.015), and channel capacity losses (0.19 bits/s/Hz) with a diversity gain of 9.91 dB. Owing to these features, the proposed CP MIMO antenna can be a good candidate for 5G systems.

REFERENCES

[1] R. Vannithamby and S. Talwar, *Towards 5G: Applications, Requirements and Candidate Technologies*. Hoboken, NJ, USA: Wiley, 2017.
[2] T. S. Rappaport, S. Sun, R. Mayzus, H. Zhao, Y. Azar, K. Wang, G. N. Wong, J. K. Schulz, M. Samimi, and F. Gutierrez, "Millimeter wave mobile communications for 5G cellular: It will work!," *IEEE Access*, vol. 1, pp. 335–349, 2013.
[3] Qualcomm Technologies Inc. (Dec. 2017). *Spectrum for 4G and 5G*. Accessed: Apr. 30, 2020. [Online]. Available: https://www.qualcomm.com/news/media-center
[4] European 5G Observatory. *National 5G Spectrum Assignment*. Accessed: May 10, 2020. [Online]. [Online]. Available: https://5gobservatory.eu/
[5] M. H. Dahri, M. I. Abbasi, M. H. Jamaluddin, and M. R. Kamarudin, "A review of high gain and high efficiency reflectarrays for 5G communications," *IEEE Access*, vol. 6, pp. 5973–5985, 2018.
[6] H. Attia, M. L. Abdelghani, and T. A. Denidni, "Wideband and high-gain millimeter-wave antenna based on FSS Fabry–Perot cavity," *IEEE Trans. Antennas Propag.*, vol. 65, no. 10, pp. 5589–5594, Oct. 2017.
[7] J. Kim, S. C. Song, H. Shin, and Y. B. Park, "Radiation from a millimeter-wave rectangular waveguide slot array antenna enclosed by a von karman radome," *J. Electromagn. Eng. Sci.*, vol. 18, no. 3, pp. 154–159, Jul. 2018.
[8] N. Nguyen-Trong, H. H. Tran, T. K. Nguyen, and A. M. Abbosh, "A compact wideband circular polarized Fabry–Perot antenna using resonance structure of thin dielectric slabs," *IEEE Access*, vol. 6, pp. 56333–56339, 2018.
[9] Q. Wei Lin, H. Wong, X. Yin Zhang, and H. Wah Lai, "Printed meandering probe-fed circularly polarized patch antenna with wide bandwidth," *IEEE Antennas Wireless Propag. Lett.*, vol. 13, pp. 654–657, 2014.
[10] H. Wong, Q. Wei Lin, H. Wah Lai, and X. Yin Zhang, "Substrate integrated meandering probe-fed patch antennas for wideband wireless devices," *IEEE Trans. Compon., Packag., Manuf. Technol.*, vol. 5, no. 3, pp. 381–388, Mar. 2015.
[11] B. T. Malik, V. Doychinov, S. A. R. Zaidi, I. D. Robertson, and N. Somjit, "Antenna gain enhancement by using low-infill 3D-printed dielectric lens antennas," *IEEE Access*, vol. 7, pp. 102467–102476, 2019.
[12] N. Hussain, T. K. Nguyen, H. Han, and I. Park, "Minimum lens size supporting the leaky-wave nature of slit dipole antenna at terahertz frequency," *Int. J. Antennas Propag.*, vol. 2016, Sep. 2016, Art. no. 5826957.
[13] S. Ghosh and D. Sen, "An inclusive survey on array antenna design for millimeter-wave communications," *IEEE Access*, vol. 7, pp. 83137–83161, 2019.
[14] H. Ullah and F. A. Tahir, "A high gain and wideband narrow-beam antenna for 5G millimeter-wave applications," *IEEE Access*, vol. 8, pp. 29430–29434, 2020.
[15] Z. Song, H. Zheng, M. Wang, E. Li, and Y. Li, "Design of one-eighth spherical dielectric resonator antenna for 5G applications," *IEEE Access*, vol. 8, pp. 9480–9487, 2020.
[16] H. N. Chen, J.-M. Song, and J.-D. Park, "A compact circularly polarized MIMO dielectric resonator antenna over electromagnetic band-gap surface for 5G applications," *IEEE Access*, vol. 7, pp. 140889–140898, 2019.

[17] A. Perron, T. A. Denidni, and A. R. Sebak, "Circularly polarized microstrip/elliptical dielectric ring resonator antenna for millimeter-wave applications," *IEEE Antennas Wireless Propag. Lett.*, vol. 9, pp. 783–786, 2010.

[18] M. Faenzi, G. Minatti, D. González-Ovejero, F. Caminita, E. Martini, C. Della Giovampaola, and S. Maci, "Metasurface antennas: New models, applications and realizations," *Sci. Rep.*, vol. 9, no. 1, pp. 1–14, Dec. 2019.

[19] J. A. Sheersha, N. Nasimuddin, and A. Alphones, "A high gain wideband circularly polarized antenna with asymmetric metasurface," *Int. J. RF Microw. Comput.-Aided Eng.*, vol. 29, no. 7, Jul. 2019, Art. no. e21740.

[20] P. K. T. Rajanna, K. Rudramuni, and K. Kandasamy, "A wideband circularly polarized slot antenna backed by a frequency selective surface," *J. Electromagn. Eng. Sci.*, vol. 19, no. 3, pp. 166–171, Jul. 2019.

[21] M. J. Jeong, N. Hussain, J. W. Park, S. G. Park, S. Y. Rhee, and N. Kim, "Millimeter-wave microstrip patch antenna using vertically coupled split ring metaplate for gain enhancement," *Microw. Opt. Technol. Lett.*, vol. 6, no. 10, pp. 2360–2365, 2019.

[22] J. Hu, G. Q. Luo, and Z.-C. Hao, "A wideband quad-polarization reconfigurable metasurface antenna," *IEEE Access*, vol. 6, pp. 6130–6137, 2018.

[23] J. Park, M. Jeong, N. Hussain, S. Rhee, S. Park, and N. Kim, "A low-profile high-gain filtering antenna for fifth generation systems based on nonuniform metasurface," *Microw. Opt. Technol. Lett.*, vol. 61, no. 11, pp. 2513–2519, 2019.

[24] N. Hussain and I. Park, "Performance of multiple-feed metasurface antennas with different numbers of patch cells and different substrate thicknesses," *Appl. Comput. Electromagn. J.*, vol. 33, no. 1, pp. 49–55, 2018.

[25] Y. M. Pan, P. F. Hu, X. Y. Zhang, and S. Y. Zheng, "A low-profile high-gain and wideband filtering antenna with metasurface," *IEEE Trans. Antennas Propag.*, vol. 64, no. 5, pp. 2010–2016, May 2016.

[26] N. Hussain, M.-J. Jeong, A. Abbas, T.-J. Kim, and N. Kim, "A metasurface-based low-profile wideband circularly polarized patch antenna for 5G millimeter-wave systems," *IEEE Access*, vol. 8, pp. 22127–22135, 2020.

[27] Q. Zheng, C. Guo, J. Ding, and G. A. E. Vandenbosch, "Dual-band metasurface-based CP low-profile patch antenna with parasitic elements," *IET Microw., Antennas Propag.*, vol. 13, no. 13, pp. 2360–2364, Oct. 2019.

[28] W. E. I. Liu, Z. N. Chen, and X. Qing, "Broadband low-profile L-Probe fed metasurface antenna with TM leaky wave and TE surface wave resonances," *IEEE Trans. Antennas Propag.*, vol. 68, no. 3, pp. 1348–1355, Mar. 2020.

[29] S. X. Ta and I. Park, "Low-profile broadband circularly polarized patch antenna using metasurface," *IEEE Trans. Antennas Propag.*, vol. 63, no. 12, pp. 5929–5934, Dec. 2015.

[30] F. Costa, O. Luukkonen, C. R. Simovski, A. Monorchio, S. A. Tretyakov, and P. M. de Maagt, "TE surface wave resonances on high-impedance surface based antennas: Analysis and modeling," *IEEE Trans. Antennas Propag.*, vol. 59, no. 10, pp. 3588–3596, Oct. 2011.

[31] K. D. Xu, H. Xu, Y. Liu, J. Li, and Q. H. Liu, "Microstrip patch antennas with multiple parasitic patches and shorting vias for bandwidth enhancement," *IEEE Access*, vol. 6, pp. 11624–11633, 2018.

[32] M. S. Alharbi, C. A. Balanis, and C. R. Birtcher, "Performance enhancement of square-ring antennas exploiting surface-wave metasurfaces," *IEEE Antennas Wireless Propag. Lett.*, vol. 18, no. 10, pp. 1991–1995, Oct. 2019.

[33] J. Wu, Y. Yin, Z. Wang, and R. Lian, "Broadband circularly polarized patch antenna with parasitic strips," *IEEE Antennas Wireless Propag. Lett.*, vol. 14, pp. 559–562, 2015.

[34] Z. Liang, J. Ouyang, and F. Yang, "Low-profile wideband circularly polarised single-layer metasurface antenna," *Electron. Lett.*, vol. 54, no. 24, pp. 1362–1364, 2018.

[35] Z.-J. Yang, L. Zhu, and S. Xiao, "An implantable wideband circularly polarized microstrip patch antenna via two pairs of degenerate modes," *IEEE Access*, vol. 7, pp. 4239–4247, 2019.

[36] J.-F. Lin and Q.-X. Chu, "Enhancing bandwidth of CP microstrip antenna by using parasitic patches in annular sector shapes to control electric field components," *IEEE Antennas Wireless Propag. Lett.*, vol. 17, no. 5, pp. 924–927, May 2018.

[37] L. Lu, G. Y. Li, A. L. Swindlehurst, A. Ashikhmin, and R. Zhang, "An overview of massive MIMO: Benefits and challenges," *IEEE J. Sel. Topics Signal Process.*, vol. 8, no. 5, pp. 742–758, Oct. 2014.

[38] A. R. Saad and H. A. Mohamed, "Printed millimeter-wave MIMO-based slot antenna arrays for 5G networks," *AEU-Int. J. Electron. Commun.*, vol. 99, pp. 59–69, Feb. 2019.

[39] B. Yang, Z. Yu, Y. Dong, J. Zhou, and W. Hong, "Compact tapered slot antenna array for 5G millimeter-wave massive MIMO systems," *IEEE Trans. Antennas Propag.*, vol. 65, no. 12, pp. 6721–6727, Dec. 2017.

[40] S. Gupta, Z. Briqech, A. R. Sebak, and T. Ahmed Denidni, "Mutual-coupling reduction using metasurface corrugations for 28 GHz MIMO applications," *IEEE Antennas Wireless Propag. Lett.*, vol. 16, pp. 2763–2766, 2017.

[41] H. T. Chattha, "4-port 2-Element MIMO antenna for 5G portable applications," *IEEE Access*, vol. 7, pp. 96516–96520, 2019.

[42] Y. Zhang, J.-Y. Deng, M.-J. Li, D. Sun, and L.-X. Guo, "A MIMO dielectric resonator antenna with improved isolation for 5G mm-wave applications," *IEEE Antennas Wireless Propag. Lett.*, vol. 18, no. 4, pp. 747–751, Apr. 2019.

[43] S. Alkaraki and Y. Gao, "Mm-wave low-cost 3D printed MIMO antennas with beam switching capabilities for 5G communication systems," *IEEE Access*, vol. 8, pp. 32531–32541, 2020.

[44] M. Khalid, S. I. Naqvi, N. Hussain, and M. U. Rahman, "4-Port MIMO antenna with defected ground structure for 5G millimeter wave applications," *Electronics*, vol. 9, no. 1, p. 71, 2020.

[45] A. Iqbal, A. Basir, A. Smida, N. K. Mallat, I. Elfergani, J. Rodriguez, and S. Kim, "Electromagnetic bandgap backed millimeter-wave MIMO antenna for wearable applications," *IEEE Access*, vol. 7, pp. 111135–111144, 2019.

[46] N. Shoaib, S. Shoaib, R. Y. Khattak, I. Shoaib, X. Chen, and A. Perwaiz, "MIMO antennas for smart 5G devices," *IEEE Access*, vol. 6, pp. 77014–77021, 2018.

[47] S. F. Jilani and A. Alomainy, "Millimetre-wave T-shaped MIMO antenna with defected ground structures for 5G cellular networks," *IET Microw., Antennas Propag.*, vol. 12, no. 5, pp. 672–677, Apr. 2018.

[48] M. Akbari, H. Abo Ghalyon, M. Farahani, A.-R. Sebak, and T. A. Denidni, "Spatially decoupling of CP antennas based on FSS for 30-GHz MIMO systems," *IEEE Access*, vol. 5, pp. 6527–6537, 2017.

[49] N. Hussain, M.-J. Jeong, J. Park, and N. Kim, "A broadband circularly polarized Fabry–Perot resonant antenna using a single-layered PRS for 5G MIMO applications," *IEEE Access*, vol. 7, pp. 42897–42907, 2019.

[50] K. R. Mahmoud and A. M. Montaser, "Synthesis of multi-polarised upside conical frustum array antenna for 5G mm-wave base station at 28/38 GHz," *IET Microw., Antennas Propag.*, vol. 12, no. 9, pp. 1559–1569, Jul. 2018.

[51] M. Mantash and T. A. Denidni, "CP antenna array with switching-beam capability using electromagnetic periodic structures for 5G applications," *IEEE Access*, vol. 7, pp. 26192–26199, 2019.

[52] A. Dadgarpour, M. Sharifi Sorkherizi, and A. A. Kishk, "High-efficient circularly polarized magnetoelectric dipole antenna for 5G applications using dual-polarized split-ring resonator lens," *IEEE Trans. Antennas Propag.*, vol. 65, no. 8, pp. 4263–4267, Aug. 2017.

[53] M.-D. Yang, Y.-M. Pan, Y.-X. Sun, and K.-W. Leung, "Wideband circularly polarized substrate-integrated embedded dielectric resonator antenna for millimeter-wave applications," *IEEE Trans. Antennas Propag.*, vol. 68, no. 2, pp. 1145–1150, Feb. 2020.

[54] W. Lin, R. W. Ziolkowski, and T. C. Baum, "28 GHz compact omnidirectional circularly polarized antenna for Device-to-Device communications in the future 5G systems," *IEEE Trans. Antennas Propag.*, vol. 65, no. 12, pp. 6904–6914, Dec. 2017.

[55] A. Iqbal, O. Saraereh, A. Bouazizi, and A. Basir, "Metamaterial-based highly isolated MIMO antenna for portable wireless applications," *Electronics*, vol. 7, no. 10, p. 267, 2018.

[56] *The Antenna Measurement System*. Accessed: May 25, 2020. [Online]. Available: https://www.emti.or.kr/index.jsp

NIAMAT HUSSAIN (Graduate Student Member, IEEE) received the B.S. degree in electronics engineering from the Dawood University of Engineering and Technology, Karachi, Pakistan, in 2014, and the M.S. degree in electrical and computer engineering from Ajou University, Suwon, South Korea. He is currently pursuing the Ph.D. degree in information and communication engineering with Chungbuk National University, Chungju, South Korea. His main research interests include lens-coupled antennas, metasurface antennas, metamaterial antennas, UWB antennas, mm-wave antennas, and terahertz antennas. He received the Best Paper Award from the Korea Winter Conference, in 2017.

MIN-JOO JEONG received the B.S. degree in electronics engineering from Chosun University, in 2013, and the M.S. degree in LED fusion engineering from Pukyong National University, South Korea, in 2015. He is currently pursuing the Ph.D. degree in information and communication engineering with Chungbuk National University, Chungju, South Korea. His research interests include EMC, antenna design, and EMF.

ANEES ABBAS received the bachelor's degree in telecommunication engineering from BUTEMS, Quetta, Pakistan, in 2014. He is currently pursuing the master's degree with the Department of Information and Communication Engineering, Chungbuk National University, South Korea. His research interests include antenna design for wifi and mobile communication.

NAM KIM received the B.S., M.S., and Ph.D. degrees in electronics engineering from Yonsei University, Seoul, South Korea, in 1981, 1983, and 1988, respectively. He has been a Professor with the School of Information and Communication Engineering, Chungbuk National University, Chengju, South Korea, since 1989. His scientific research interests include optical information processing, health effect of the EMF, wireless power transfer, and antennas for mobile communications. He was the President of the Bioelectromagnetics Society. He is a member with the International Advisory Committee, World Health Organization Project on EMF, the IEEE International Committee on Electromagnetic Safety, and the International Electro Technical Commission TC 106.